LETTERS

A crystallizing dense magma ocean at the base of the Earth's mantle

S. Labrosse[1], J. W. Hernlund[2]† & N. Coltice[1,3]

The distribution of geochemical species in the Earth's interior is largely controlled by fractional melting and crystallization processes that are intimately linked to the thermal state and evolution of the mantle. The existence of patches of dense partial melt at the base of the Earth's mantle[1], together with estimates of melting temperatures for deep mantle phases[2] and the amount of cooling of the underlying core required to maintain a geodynamo throughout much of the Earth's history[3], suggest that more extensive deep melting occurred in the past. Here we show that a stable layer of dense melt formed at the base of the mantle early in the Earth's history would have undergone slow fractional crystallization, and would be an ideal candidate for an unsampled geochemical reservoir hosting a variety of incompatible species (most notably the missing budget of heat-producing elements) for an initial basal magma ocean thickness of about 1,000 km. Differences in $^{142}Nd/^{144}Nd$ ratios between chondrites and terrestrial rocks[4] can be explained by fractional crystallization with a decay timescale of the order of 1 Gyr. These combined constraints yield thermal evolution models in which radiogenic heat production and latent heat exchange prevent early cooling of the core and possibly delay the onset of the geodynamo to 3.4–4 Gyr ago[5].

The survival of a layer of melt formed at the base of the Earth's mantle early in its history (Fig. 1a) will have depended on whether it was both gravitationally and chemically stable. Gravitational stability is satisfied if the melt formed in Earth's deep mantle is more dense than mantle solids on account of a modest enrichment in iron relative to magnesium and a small[6] or negative[7] molar volume change for silicate melting at high pressures. The low viscosity of such a melt layer ensures vigorous convection and mixing that maintains nearly isentropic conditions (Supplementary Information) and provides a large effective volume for chemical interaction with the core. Thus the chemical stability of a basal melt layer largely hinges on the capacity of the core to come to equilibrium without entirely consuming the layer or removing those chemical components that allow the layer to remain gravitationally stable.

Assuming stability of such a primordial basal melt layer, a simple model for its evolution coupled to the core and the overlying solid mantle can be constructed by assuming an isentropic temperature in the melt layer, an isentropic core[3], and a thermal boundary layer at the base of the solid mantle in which the temperature varies linearly with depth (Fig. 2a):

$$4\pi a^2 k \frac{T_L - T_M}{\delta} = -\left(M_m C_{pm} + M_C C_{pC}\right)\frac{dT_L}{dt} + H(t) - 4\pi a^2 \rho \Delta S T_L \frac{da}{dt} \quad (1)$$

with a the upper radius of the melt layer, T_L its liquidus temperature, T_M the temperature above the solid mantle boundary layer, δ the thickness of the boundary layer (assumed constant; Supplementary Information), M_m and M_C the respective masses of the melt layer and

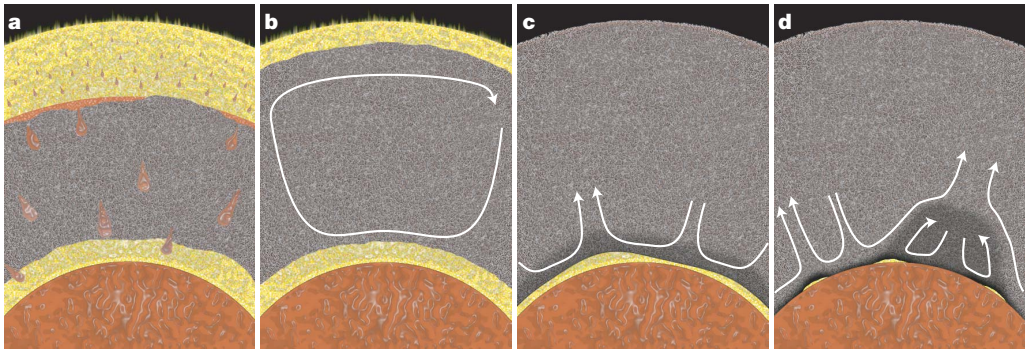

Figure 1 | Schematic illustration of the formation and evolution of a dense basal magma ocean. a, Iron-rich liquid descends as a rain of droplets in the shallower magma ocean, accumulates on top of the solid mantle and undergoes diapiric instability and rapid transport to the core. **b**, The molten layers formed at the top and bottom of the mantle crystallize, and deposit material onto a solid mantle layer that grows upward at the top and downward at the bottom at two vastly different rates. **c**, After the surface magma ocean has fully crystallized, the slowly cooling basal melt layer fractionally crystallizes increasingly Fe-enriched solids that are deposited upwards onto the bottom of the solid mantle. **d**, After a substantial part of the basal magma ocean has frozen, the solid that forms may itself contain enough dense components to become stable against complete entrainment in the solid mantle, hence forming piles under upwelling currents. The remaining thin mushy layer of melt is thicker where mantle flow converges along the core–mantle boundary, leading to seismically detectable ultralow-velocity zones. Solid-state convection in the mantle (white arrows in **b**, **c**, **d**) controls the rate of crystallization of the bottom magma ocean and the possible entrainment of FeO-enriched dense material accumulating at the base of the solid mantle (dark grey in **c** and **d**).

[1]Laboratoire des sciences de la Terre, Ecole Normale Supérieure de Lyon, Université de Lyon, CNRS UMR 5570, 46 Allée d'Italie, 69364 Lyon Cedex 07, France. [2]Équipe de Dynamique des Fluides Géologiques, Institut de Physique du Globe de Paris, 4 place Jussieu, 75252 Paris Cedex 05, France. [3]Laboratoire des sciences de la Terres, Université Lyon 1, Université de Lyon, CNRS UMR 5570, 2 rue Raphael Dubois, 69622 Villeurbanne Cedex, France. †Present address: Department of Earth and Ocean Sciences, University of British Columbia, Vancouver, BC V6T 1Z4, Canada.

the core, C_{pm} and C_{pC} their respective specific heats, H the radiogenic heat production in the layer, ρ the density of the melt, k the thermal conductivity of the solid mantle, and ΔS the specific entropy of melting.

Recent shock measurements suggest that a deep melt layer will maintain a relatively large adiabatic gradient relative to the change in liquidus temperature with depth, which would ensure that crystallization should proceed downward from the top of the layer on cooling[7]. The thermal evolution is coupled to the crystallization of the melt layer via the phase diagram, which is not well constrained for the deep mantle. For purposes of illustration, we use an idealized solid-solution (Fig. 2b), where an MgO-rich end-member (denoted A) has a higher melting temperature T_A than the melting temperature T_B of a dense FeO-rich component (denoted B). On fractional crystallization, the melt is gradually enriched in component B, and denoting by ξ_L and ξ_S the mass fraction of B in the melt and the solid, respectively, conservation of chemical species gives:

$$\frac{d\xi_L}{dt} = -\frac{3a^2\Delta\xi}{a^3 - b^3}\frac{da}{dt} \quad (2)$$

with $\Delta\xi = \xi_L - \xi_S$ the enrichment of the melt in the dense component relative to the solid, and b the radius of the core. The linearized phase diagram is used to relate $d\xi_L/dt$ to dT_L/dt, and we obtain two coupled equations for T_L and a that can be solved numerically from any time where both quantities are known.

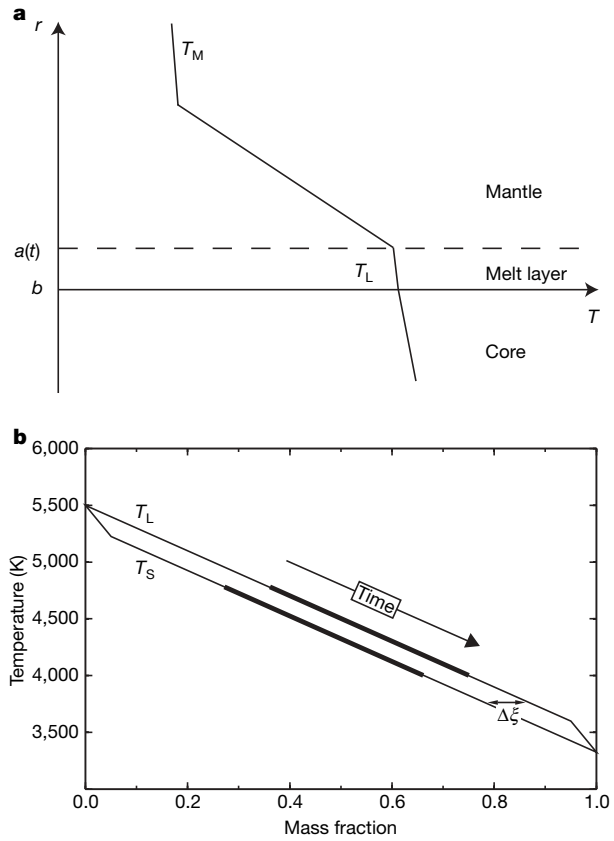

Figure 2 | Sketch of the idealized model. **a**, Model for the decrease of temperature T as function of radius r, with isentropic profiles in the core ($r < b$) and melt layer ($b < r < a(t)$) up to the liquidus temperature of mantle material T_L at the freezing interface, overlaid by a boundary layer in the solid mantle ($r > a(t)$) where the temperature decreases linearly with radius to reach the lower mantle temperature T_M. **b**, Idealized phase diagram for a solid solution, for example $Mg_xFe_{1-x}O$ or $Mg_xFe_{1-x}SiO_3$, the liquidus and solidus temperature T_L and T_S having $\Delta\xi$ as difference in mass fraction of the light component. The thickened lines represent the region of the phase diagram that is covered during the evolution presented in Fig. 3.

In this idealized case, the thickness of the melt layer decreases exponentially with time while the temperature decreases linearly (Fig. 3), consistent with an approximate analytic solution for $a - b \ll b$ and a constant cooling timescale of $\tau_C = M_C C_{pC}\Delta\xi(T_A - T_B)/(4\pi b^2 k(T_L - T_M)/\delta - H)$, as suggested by the energy balance (Fig. 3). In this case, τ_C is the e-fold time for the decay of the layer thickness, and $\Delta\xi(T_A - T_B)/\tau_C$ is the linear decay constant for the temperature. It is primarily controlled by the product of the heat capacity of the core and the temperature range $(T_A - T_B)$ over which a liquid can exist in the phase diagram. Although the

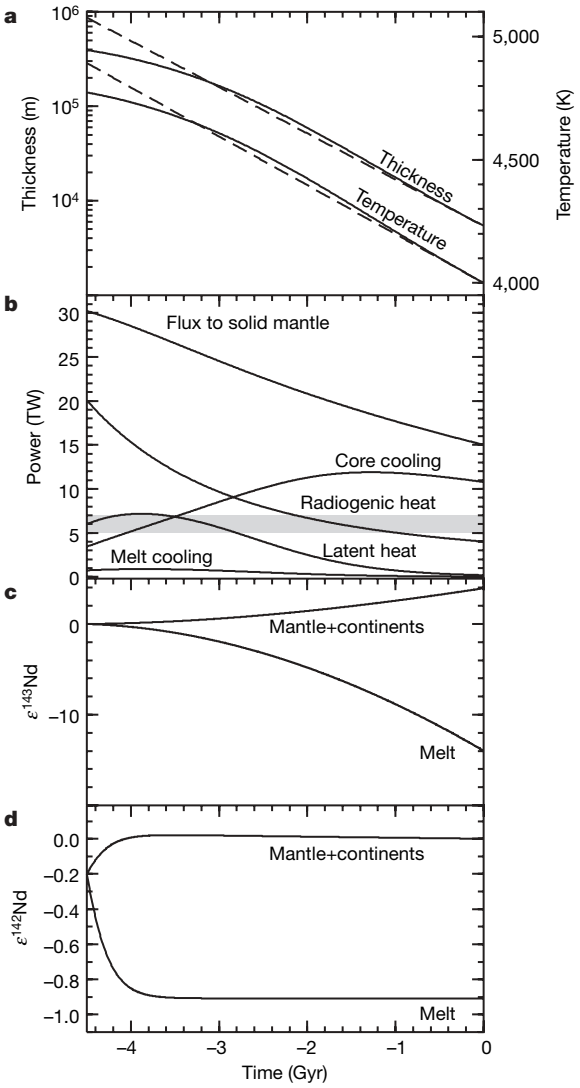

Figure 3 | Evolution of the preferred model as a function of time. **a**, Thickness (left scale), and temperature (right scale) of the melt layer. **b**, Energy budget. **c**, **d**, ε^{143}Nd (**c**) and ε^{142}Nd (**d**) of the solid and melt reservoirs predicted by the model of crystallization of the basal magma ocean. The solid lines in **a** and **b** are obtained by numerical integration of equations (1) and (2), whereas the dashed lines are a corresponding approximate analytic solution (Supplementary Information). The light grey area in **b** gives the range of core cooling that must be exceeded in order to support thermal convection in the core, and shows that the onset of the geodynamo is delayed to 4–3.4 Gyr ago in this example. The Sm–Nd calculations are made using $D_{Sm} = 0.05$, $D_{Nd} = 0.02$ (ref. 18) for partition coefficients between melt and solid for Sm and Nd, an initial mass of melt $M_{mi} = 0.78 \times 10^{24}$ kg, a decay timescale for the melt $\tau_C = 887$ Myr, an initial melt fraction $F = 0.8$ and a time of magma ocean formation after formation of calcium aluminium inclusions (CAIs) $t_i = 30$ Myr, corresponding to the thermal evolution shown in **a** and **b**. Other parameters for the thermal evolution model are given in Supplementary Information.

physical parameters appearing in this problem are ill-constrained, an order-of-magnitude estimate yields τ_C of the order of 1 Gyr.

Chemical interaction with the core is neglected in this simple example, although it might be expected to have an important effect on the evolution of the melt layer. For example, an enrichment in iron oxides inside the silicate melt layer with time may favour the formation of FeO and FeSi (ref. 8) liquids when reacted with metallic Fe; these products may or may not be miscible in the core, depending on whether or not it is initially saturated or whether a stratified light-element-enriched layer forms at the top of the core[9]. Removal of such products into the core could accelerate freezing of the basal layer, by consuming a presumed low-melting-temperature Fe-rich component in the melt. On the other hand, cooling of a core whose surface is saturated would favour expulsion of light elements from the core if they become relatively less soluble in metallic Fe as temperature decreases[10]; such expulsion could possibly enrich the melt layer in low-melting-temperature components via the reverse reaction and prolong its crystallization. Although the equilibrium processes governing this kind of interaction are not well known, and also depend on a variety of unknown initial conditions that are set by the formation of the core in the early Earth, the plausibility of a slowly crystallizing basal melt layer can additionally be evaluated using other independent constraints.

Fractional crystallization of a large body of liquid in the deep mantle will have important consequences for the distribution of chemical species in Earth's mantle. It is well known that the continental crust and the depleted mantle are not geochemically complementary to one another with respect to the entire mass of Earth's mantle. In particular, if the Earth has a chondritic composition for refractory elements, about 20–30% of the budget of very incompatible elements (and hence heat-producing species such as uranium, thorium and potassium) must be sequestered in a 'hidden reservoir'[11], such as a pristine layer in the lower mantle[12], or in a D″ layer made of segregated oceanic crust[13]. The mass balance of coupled ^{40}K and ^{40}Ar requires that the hidden reservoir, rich in ^{40}K, also contains 20–60% of the ^{40}Ar budget[14]. As a consequence, this reservoir must have remained undegassed for several billion years; however, it cannot be pristine as its Nb/Ta and Nb/La ratios must be higher than those of the bulk silicate Earth[15,16]. Because Nb is more incompatible than Ta and La, the hidden reservoir should be derived from a melt. Additionally, every measured Earth sample has excess ^{142}Nd ($\varepsilon^{142}\mathrm{Nd} \geq 0$) relative to chondrites ($\varepsilon^{142}\mathrm{Nd}$ of -0.2)[4]. As the Earth is expected to be chondritic for refractory elements, the ^{142}Nd signature of sampled rocks has to be balanced by a hidden and unsampled reservoir in the deep mantle having an even more negative ε^{142}Nd and a low Sm/Nd ratio. The hidden reservoir has to be formed within the first 100 Myr of Earth's history at most, because ^{142}Nd is produced by decay of ^{146}Sm with a half-life of 103 Myr (ref. 17).

The basal magma ocean is a unique candidate for the hidden geochemical reservoir. Therefore, we can use the balance of incompatible elements in addition to ^{142}Nd/^{144}Nd and ^{143}Nd/^{144}Nd data to constrain its thermal evolution. We take partition coefficients between $(Mg,Fe)SiO_3$ perovskite (the assumed liquidus phase) and melt from experimental results[18]. Using an exponentially decaying mass for the melt layer as discussed previously, we solve analytically the evolution of the whole Sm–Nd system constrained by the observed present-day ^{142}Nd/^{144}Nd and ^{143}Nd/^{144}Nd ratios of the bulk mantle (Supplementary Information and Fig. 3) starting from a chondritic Earth. Because the melt is denser and much less viscous than the overlying solid mantle, entrainment into the mantle is negligible and therefore the geochemical signal of the melt layer is unsampled[17]. Models predicting 20–30% of the total chondritic uranium budget in the deep melt today and realistic present-day values of ^{142}Nd/^{144}Nd and ^{143}Nd/^{144}Nd for the solid mantle require an initial 850 ± 150 km thick basal magma ocean to be extracted by 80 ± 5% melting of the lowermost mantle (Supplementary Information). The residue of melting ultimately mixes back into the overlying solid mantle (Fig. 1b, c). Nevertheless, fractional crystallization produces crystals that are highly depleted in incompatible elements and returns a Sm/Nd signal that is very dilute with respect to the overall mantle. Predictions can be made for the composition of the solid mantle and the underlying melt layer using the above geochemical constraints. The initial composition of the melt is computed from 80% batch melting of primitive mantle[19] to produce a melt layer 850 km thick. With a fractional crystallization model, we obtain the present-day composition of the melt, which is slightly richer in incompatible elements than the continental crust (Fig. 4) and accounts for about 20% of the total budget. Applying a mass balance with the continental crust[20] and the remaining melt, we can then predict a composition of the solid mantle (Fig. 4) that is consistent with estimates of the shallow mantle[21] and with the trace-element pattern of normal mid-ocean-ridge basalts[22].

The crystallizing solids can exhibit increased Fe/Mg with time because of magma differentiation, and eventually their intrinsic density excess relative to the overlying mantle may become large enough to stabilize them against entrainment by mantle convection[12]. In this scenario, the shape of the denser crystalline piles is determined by the viscous coupling with the overlying mantle, with downgoing slabs pushing aside the Fe-rich rocks that tend to accumulate under upwelling currents. The existence of such piles has already been inferred from seismological studies[23], in which a counter-circulation developing within them tends to sweep residual melt to their edges[24] (Fig. 1d). A small fraction of the dense cumulates can be entrained but this should produce no geochemical signal, as incompatible elements stay within the melt rather than within the cumulates. Noble gases may constitute an exception because of the intense outgassing that occurred at the surface of the overlying solid mantle (more than 99% degassing for non-radiogenic helium, neon and argon[25]).

Another implication of the basal magma ocean is that the heat flow into the solid mantle has a contribution from heat production in the melt layer, in addition to the cooling of the core (equation (1)).

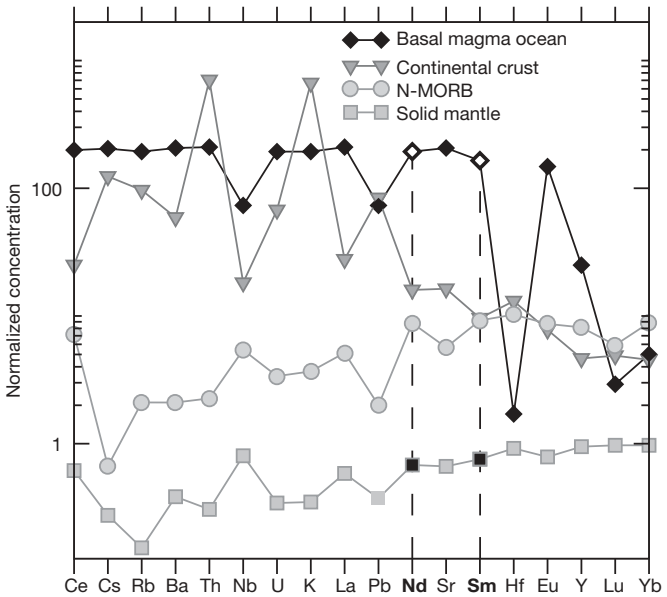

Figure 4 | Predicted element concentrations in the present-day basal magma ocean and solid mantle. Also shown for comparison are patterns for the continental crust[20] and the average normal mid-ocean-ridge basalt (N-MORB)[22]. All concentrations have been normalized by those of the bulk silicate Earth[19]. The present concentration in the melt results from fractional crystallization (calculated using the partition coefficients of ref. 18) and a solid mantle composition calculated from mass balance with the continental crust and the basal magma ocean. Nd and Sm are emphasized to highlight their difference in partition coefficients, responsible for the evolution of ^{142}Nd and ^{143}Nd (Fig. 3).

Hence, estimates of core cooling from seismic observations of a double-crossing of the post-perovskite phase boundary[26,27] might be revised to lower values by up to 4–6 TW. More importantly, both radiogenic heating and the contribution from latent heat of crystallization were significantly larger in the early Earth, limiting core heat loss to values lower than the minimal value (5–7 TW) required for thermal convection (Fig. 3). As the inner core would only appear around 1 Gyr ago with such a thermal history[3], the early geodynamo cannot be supported by compositional convection and can only start at the onset of thermal convection, between 4 and 3.4 Gyr ago. The delayed onset of the geodynamo would allow implantation of some of Earth's early atmosphere in lunar soil[5], and is consistent with the oldest known palaeomagnetic record[28].

Received 21 May; accepted 2 October 2007.

1. Williams, Q. & Garnero, E. J. Seismic evidence for partial melt at the base of the Earth's mantle. *Science* **273,** 1528–1530 (1996).
2. Zerr, A., Diegeler, A. & Boehler, R. Solidus of Earth's deep mantle. *Science* **281,** 243–246 (1998).
3. Labrosse, S. Thermal and magnetic evolution of the Earth's core. *Phys. Earth Planet. Inter* **140,** 127–143 (2003).
4. Boyet, M. & Carlson, R. W. ^{142}Nd Evidence for early (> 4.53 Ga) global differentiation of the silicate Earth. *Science* **309,** 576–581 (2005).
5. Ozima, M. *et al.* Terrestrial nitrogen and noble gases in lunar soils. *Nature* **436,** 655–659 (2005).
6. Stixrude, L. & Karki, B. Structure and freezing of $MgSiO_3$ liquid in Earth's lower mantle. *Science* **310,** 297–299 (2005).
7. Mosenfelder, J. P., Asimow, P. D. & Ahrens, T. J. Thermodynamic properties of Mg_2SiO_4 liquid at ultra-high pressures for shock measurements to 200 GPa on forsterite and wadsleyite. *J. Geophys. Res.* **112,** B06208, doi:10.1029/2006JB004364 (2007).
8. Knittle, E. & Jeanloz, R. Earth's core-mantle boundary: Results of experiments at high pressures and temperatures. *Science* **251,** 1438–1443 (1991).
9. Braginsky, S. I. Dynamics of the stably stratified ocean at the top of the core. *Phys. Earth Planet. Inter* **111,** 21–34 (1999).
10. Buffett, B. A. Earth's core and the geodynamo. *Science* **288,** 2007–2012 (2000).
11. Hofmann, A. W. Mantle geochemistry: The message from oceanic volcanism. *Nature* **385,** 219–229 (1997).
12. Davaille, A. Simultaneous generation of hotspots and superswells by convection in a heterogeneous planetary mantle. *Nature* **402,** 756–760 (1999).
13. Coltice, N. & Ricard, Y. Geochemical observations and one layer mantle convection. *Earth Planet. Sci. Lett.* **174,** 125–137 (1999).
14. Allègre, C. J., Hofmann, A. & O'Nions, K. The argon constraints on mantle structure. *Geophys. Res. Lett.* **23,** 3555–3557 (1996).
15. Sun, S. S. & McDonough, W. F. in *Magmatism in the Ocean Basins* (eds Saunders, A. & Norry, M.) 313–345 (Spec. Publ. Vol. 42, Geol. Soc. Lond., 1989).
16. Rudnick, R. L., Barth, M., Horn, I. & McDonough, W. F. Rutile-bearing refractory eclogites: Missing link between continents and depleted mantle. *Science* **287,** 278–281 (2000).
17. Boyet, M. & Carlson, R. W. A new geochemical model for the Earth's mantle inferred from ^{146}Sm-^{142}Nd systematics. *Earth Planet. Sci. Lett.* **250,** 254–268 (2006).
18. Corgne, A., Liebske, C., Wood, B. J., Rubie, D. C. & Frost, D. J. Silicate perovskite-melt partitioning of trace elements and geochemical signature of a deep perovskitic reservoir. *Geochim. Cosmochim. Acta* **69,** 485–496 (2005).
19. Mcdonough, W. F. & Sun, S. S. The composition of the Earth. *Chem. Geol.* **120,** 223–253 (1995).
20. Rudnick, R. L. & Fountain, D. M. Nature and composition of the continental crust: A lower crustal perspective. *Rev. Geophys.* **33,** 267–309 (1995).
21. Salters, V. J. M. & Stracke, A. Composition of the depleted mantle. *Geochem. Geophys. Geosyst.* **5,** Q05004, doi:10.1029/2003GC000597 (2004).
22. Hofmann, A. W. Chemical differentiation of the Earth: The relationship between mantle, continental crust and oceanic crust. *Earth Planet. Sci. Lett.* **90,** 297–314 (1988).
23. Wen, L. X., Silver, P., James, D. & Kuehnel, R. Seismic evidence for a thermo-chemical boundary at the base of the Earth's mantle. *Earth Planet. Sci. Lett.* **189,** 141–153 (2001).
24. Thorne, M. S. & Garnero, E. J. Inferences on ultralow-velocity zone structure from a global analysis of SPdKS waves. *J. Geophys. Res.* **109,** B08301, doi:10.1029/2004JB003010 (2004).
25. Allègre, C. J., Staudacher, T. & Sarda, P. Rare gas systematics: Formation of the atmosphere, evolution and structure of the Earth's mantle. *Earth Planet. Sci. Lett.* **81,** 127–150 (1987).
26. Hernlund, J. W., Thomas, C. & Tackley, P. J. A doubling of the post-perovskite phase boundary and structure of the Earth's lowermost mantle. *Nature* **434,** 882–886 (2005).
27. Lay, T., Hernlund, J., Garnero, E. J. & Thorne, M. S. A post-perovskite lens and D'' heat flux beneath the central Pacific. *Science* **314,** 1272–1276 (2006).
28. Tarduno, J. A., Cottrell, R. D., Watkeys, M. K. & Bauch, D. Geomagnetic field strength 3.2 billion years ago recorded by single silicate crystals. *Nature* **446,** 657–660 (2007).

Supplementary Information is linked to the online version of the paper at www.nature.com/nature.

Acknowledgements We thank D. Stevenson for comments that helped us to considerably sharpen this paper. M. Moreira, C. Jaupart and M. Jellinek also provided valuable feedback. This research was supported by the SEDIT programme of INSU, the French Ministry of Research and a CIAR postdoctoral fellowship.

Author Contributions All authors contributed equally to the manuscript.

Author Information Reprints and permissions information is available at www.nature.com/reprints. Correspondence and requests for materials should be addressed to S.L. (stephane.labrosse@ens-lyon.fr).